

**Supporting Information**

The Distinct Photophysics Of the Isomers of B<sub>18</sub>H<sub>22</sub>  
Explained

*Michael G.S. Londenborough,<sup>\*,a</sup> Drahomir Hnyk,<sup>\*,a</sup> Jonathan Bould,<sup>a</sup> Luis Serrano-Andrés,<sup>b</sup> Vicenta Sauri,<sup>b</sup> Josep M. Oliva,<sup>\*,‡</sup> Pavel Kubát,<sup>b</sup> Tomáš Polívka,<sup>c</sup> and Kamil Lang,<sup>\*,a</sup>*

<sup>a</sup> Institute of Inorganic Chemistry of the AS CR, v.v.i., 250 68 Husinec-Řež,

Czech Republic,

<sup>b</sup> Instituto de Ciencia Molecular, Universitat de València, Valencia, Spain,

Instituto de Química Física “Rocasolano”, CSIC, Madrid, Spain,

J. Heyrovský Institute of Physical Chemistry of the AS CR, v.v.i., Dolejškova 3, 182 23 Praha 8,

Czech Republic

Institute of Physical Biology, University of South Bohemia, Zámek 136, 373 33 Nové Hrady,

Czech Republic.

AUTHOR EMAIL ADDRESS:

michaell@iic.cas.cz (M.G.S. Londenborough)

j.m.oliva@iqfr.csic.es (J.M. Oliva)

hnyk@iic.cas.cz (D. Hnyk)

lang@iic.cas.cz (K. Lang)

## Contents

Additional computational details.

**Figure S1.** UV-vis absorption and fluorescence emission spectra of *anti*-B<sub>18</sub>H<sub>22</sub> and *syn*-B<sub>18</sub>H<sub>22</sub>.

**Figure S2.** Kinetics measured at maxima of transient absorption spectra of *anti*-B<sub>18</sub>H<sub>22</sub> and *syn*-B<sub>18</sub>H<sub>22</sub>.

**Figure S3.** Phosphorescence signals of O<sub>2</sub>(<sup>1</sup>Δ<sub>g</sub>) at 1270 nm produced by *anti*-B<sub>18</sub>H<sub>22</sub> and *syn*-B<sub>18</sub>H<sub>22</sub> in air-saturated hexane.

**Figure S4.** Time dependence of the O<sub>2</sub>(<sup>1</sup>Δ<sub>g</sub>) luminiscence signal at 1275 nm produced by *anti*-B<sub>18</sub>H<sub>22</sub> in chloroform.

**Figure S5.** Boron-boron distance differences (in Å) between the energy minima geometries of groundstate S<sub>0</sub> and first triplet state T<sub>1</sub> in *anti*-B<sub>18</sub>H<sub>22</sub>.

**Figure S6.** Boron-boron distance differences (in Å) between the energy minima geometries of groundstate S<sub>0</sub> and first excited singlet state S<sub>1</sub> in *anti*-B<sub>18</sub>H<sub>22</sub>.

**Figure S7.** Boron-boron distance differences (in Å) between the energy minimum geometry of groundstate S<sub>0</sub> and conical intersection geometry (S<sub>0</sub>/S<sub>1</sub>)<sub>CI</sub> in *anti*-B<sub>18</sub>H<sub>22</sub>.

**Figure S8.** Boron-boron distance differences (in Å) between the energy minima geometries of groundstate S<sub>0</sub> and first triplet state T<sub>1</sub> in *syn*-B<sub>18</sub>H<sub>22</sub>.

**Figure S9.** Boron-boron distance differences (in Å) between the energy minimum geometry of groundstate S<sub>0</sub> and conical intersection geometry (S<sub>0</sub>/S<sub>1</sub>)<sub>CI</sub> in *syn*-B<sub>18</sub>H<sub>22</sub>.

**Table S1.** Theoretical (CASPT2) and experimental absorption spectra of *anti*-B<sub>18</sub>H<sub>22</sub> ( $C_i$ ).

**Table S2.** Theoretical (CASPT2) and experimental absorption spectra of *syn*-B<sub>18</sub>H<sub>22</sub> ( $C_2$ ).

**Table S3.** Cartesian coordinates of the optimized structure geometries at individual single points along the PEH.

**References.**

## **Additional computational details**

Most calculations reported in the present contribution have been performed using the CASPT2//CASSCF protocol, in which geometry optimizations, including minima and surface crossings were carried at the multiconfigurational CASSCF level, whereas electronic energy computations use the second-order multiconfigurational perturbation approach, CASPT2.<sup>1,2,3,4</sup> Different active spaces have been employed in order to ensure the converged character of the results. Initially, active spaces of 6 electrons and 6 orbitals (6/6) was used to optimize the minima and (2/2) to optimize the state crossings, and the results were refined using a final space of 12 electrons in 12 orbitals, finally selected by performing Restricted Active Space SCF (RASSCF) calculations, a method which allows to extend the size of active spaces by restricting the CI excitation level.<sup>5</sup> The one-electron atomic basis set 6-31+G(d) was used throughout. Test calculations, mentioned in the text, were performed by using a larger ANO-S type basis set contracted to B [3s2p1d] / H [2s1p] to analyze the effect of increasing the quality of the basis set. The results were insensitive within the expected 0.1-0.2 eV accuracy range. As an example, the transition to the  $^1\text{A}_\text{u}$ , state in the *anti*-B<sub>18</sub>H<sub>22</sub> isomer was computed at 3.82 eV (3.93 eV with 6-31+G(d)) using an ANO-S B [3s2p1d]/H [2s1p] basis set, just improving the accordance with the experimental band maxima. The new IPEA=0.25 au zeroth-order Hamiltonian was employed in the CASPT2 calculations,<sup>6</sup> which include an imaginary level-shift correction of 0.1 au in order to avoid the presence of intruder states.<sup>7</sup> All CASSCF/CASPT2 calculations used the MOLCAS-7.0 set of programs,<sup>8</sup> whereas the DFT optimizations used the Gaussian-03 program.<sup>9</sup>

The vertical absorption energies have been performed by state-average (SA)-CASSCF/CASPT2 of seven roots for the  $^1\text{A}_\text{g}$  and  $^1\text{A}$  states, six roots for  $^1\text{A}_\text{u}$  and  $^1\text{B}$ , five roots for  $^3\text{A}_\text{g}$  and  $^3\text{A}$  and four roots for the  $^3\text{A}_\text{u}$  and  $^3\text{B}$  states. The vertical emission energies have been computed by a single root calculation at the same level than the absorption energies for both singlet and triplet A<sub>u</sub> and B states. In all these calculations an active space of (12/12) is used. Table S1 and Table S2 compile the CASPT2

absorption energies and other properties together with the main configurations of the CASSCF wave functions. The experimental data are also included.

In this contribution conical intersection searches were carried out using the restricted Lagrange multipliers technique as included in the MOLCAS-7.0 package<sup>8</sup> in which the lowest-energy point was obtained under the restriction of degeneracy between the two considered states.<sup>10</sup> The surface crossings were obtained as minimum energy crossing points (MECPs), in which no non-adiabatic coupling matrix elements (NACMEs) were estimated. CASSCF convergence was accepted for energy gaps lower than 2 kcal/mol (<0.08 eV), which is a commonly assumed criterion.

Regarding the calculation of the spin-orbit coupling (SOC) elements, they were obtained as follows. In the CASSI formalism, the components of the SOC vector  $\langle T_{l,u} | \hat{H}_{SO} | S_k \rangle$  are decomposed into sums of the form:

$$\langle T_{l,u} | \hat{H}_{SO} | S_k \rangle = \sum_{p,q} \langle \phi_p | \hat{H}_{L,u} | \phi_q \rangle P_{pq}^{\alpha\beta}$$

where  $\langle \phi_p | \hat{H}_{L,u} | \phi_q \rangle$  are the spin-orbit coupling integrals in the basis of molecular orbitals, and  $P_{pq}^{\alpha\beta}$  are the transition spin density matrix elements between configurations of the active space.<sup>11</sup> The SOC strength between selected states was computed as

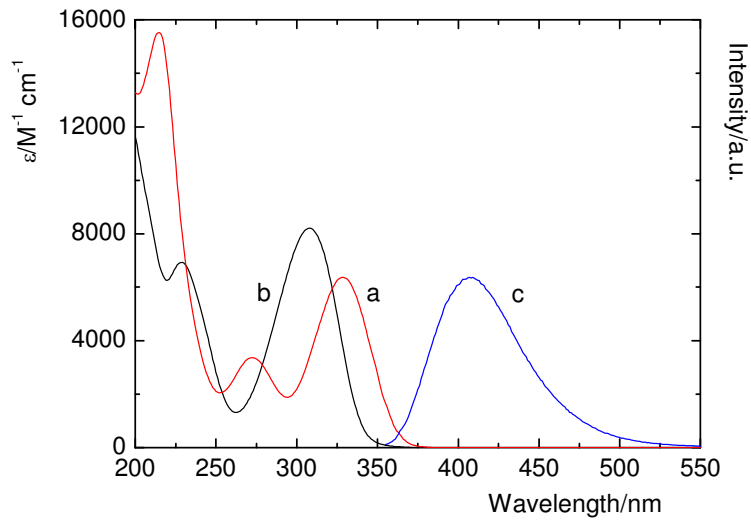
$$SOC_{lk} = \sqrt{\sum_u \left| \langle T_{l,u} | \hat{H}_{SO} | S_k \rangle \right|^2} \quad u = x, y, z$$

which can be considered the length of the spin-orbit coupling vector  $SOC_{lk}$  with component  $\langle T_{l,u} | \hat{H}_{SO} | S_k \rangle$ . The algorithms implemented in the Molcas-7 program were employed.<sup>8</sup> A CASSCF(12,12)/6-31+G(d) wave function averaged over 16 singlet and 16 triplet states was used. From the calculated CASSCF transition dipole moments (TDM) and the CASPT2 excitation energies, the radiative lifetimes have been estimated by using the Strickler-Berg relationship,<sup>12</sup> as described elsewhere.<sup>13</sup> In particular, the S-T TDMs were obtained by the following expression:

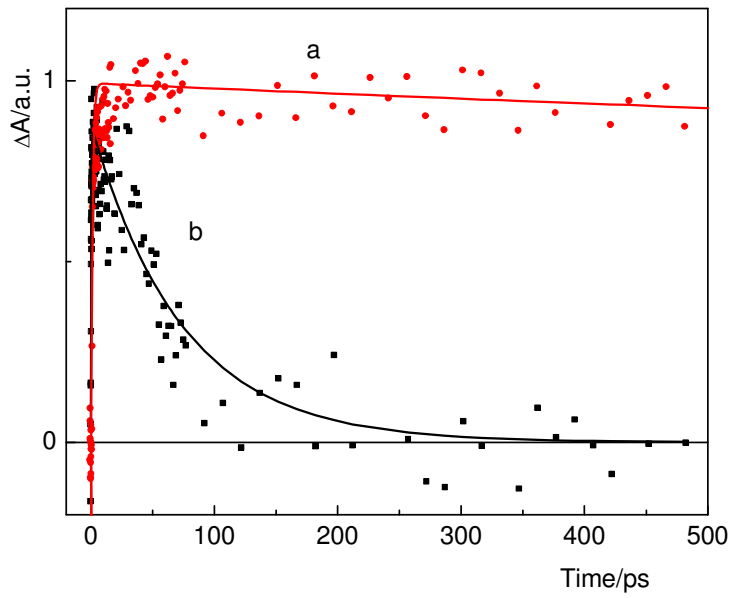
$$TDM_{ST} = \langle S|r^1|T^k\rangle = \sum_n \frac{\langle S^0|r^1|S_n^0\rangle\langle S_n^0|H_{SO}^k|T^{k,0}\rangle}{E(T^0) - E(S_n^0)} + \sum_m \frac{\langle S^0|H_{SO}^k|T_m^{k,0}\rangle\langle T_m^{k,0}|r^1|T^{k,0}\rangle}{E(S^0) - E(S_m^0)}$$

Table S3 compiles the Cartesian coordinates of the optimized minima and surface crossings obtained in the present contribution for the two octadecaborane isomers described at the DFT/B3LYP/6-31+G(d) or CASSCF(12/12)/6-31+G(d) levels of theory, and includes also absolute energies at the CASSCF level of theory.

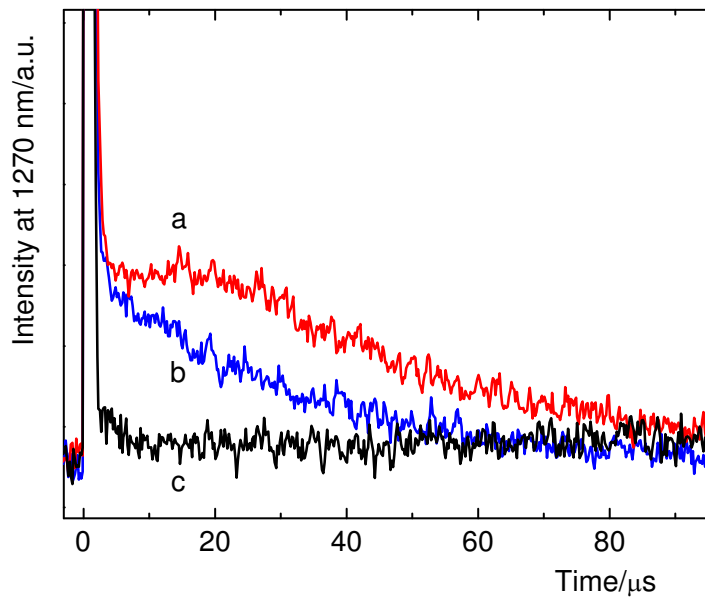
**Figure S1.** UV-vis absorption spectra of *anti*-B<sub>18</sub>H<sub>22</sub> (a, red), *syn*-B<sub>18</sub>H<sub>22</sub> (b, black) (left axis), and fluorescence emission spectra (c, blue) ( $\lambda_{\text{exc}} = 340$  nm) of *anti*-B<sub>18</sub>H<sub>22</sub> (right axis) in hexane.



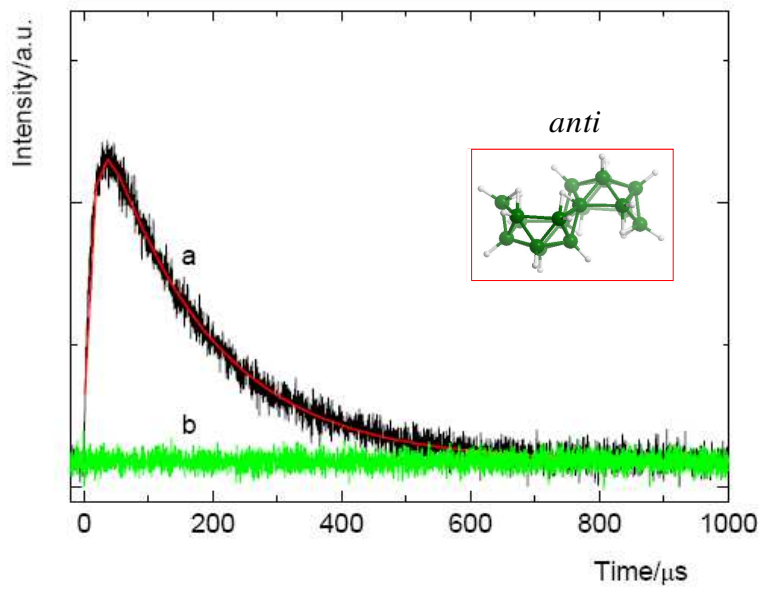
**Figure S2.** Kinetics measured at maxima of transient absorption spectra of *anti*-B<sub>18</sub>H<sub>22</sub> (a) and *syn*-B<sub>18</sub>H<sub>22</sub> (b) at 512 nm and 475 nm, respectively.



**Figure S3.** Raw phosphorescence signals of  $O_2(^1\Delta_g)$  at 1270 nm produced by *anti*- $B_{18}H_{22}$  (a) and *syn*- $B_{18}H_{22}$  (b) in air-saturated hexane are compared with a short-lived signal caused by scattering of an excitation laser pulse in oxygen-free solutions (c).



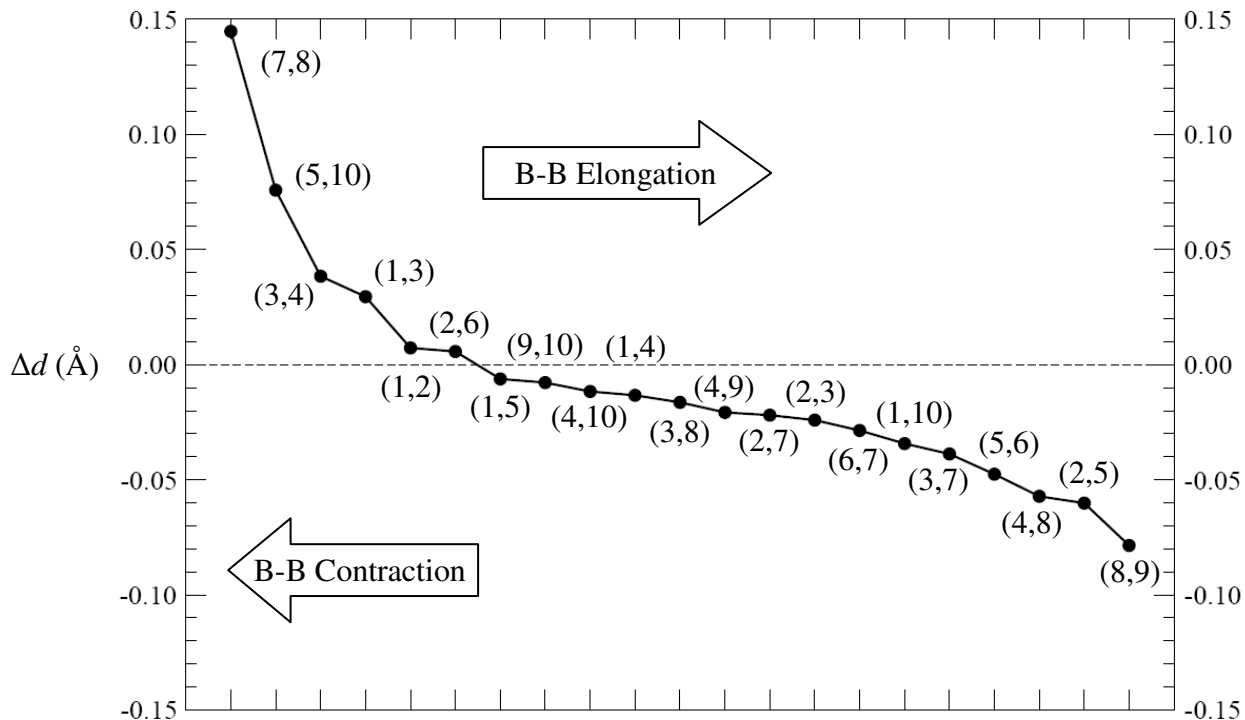
**Figure S4.** Time dependence of the  $O_2(^1\Delta_g)$  luminiscence signal at 1275 nm produced by *anti*- $B_{18}H_{22}$  in chloroform ( $\lambda_{exc} = 355$  nm): air-saturated (a) and  $N_2$ -saturated solution (b). The smoothed line (red) is a least squares fit.



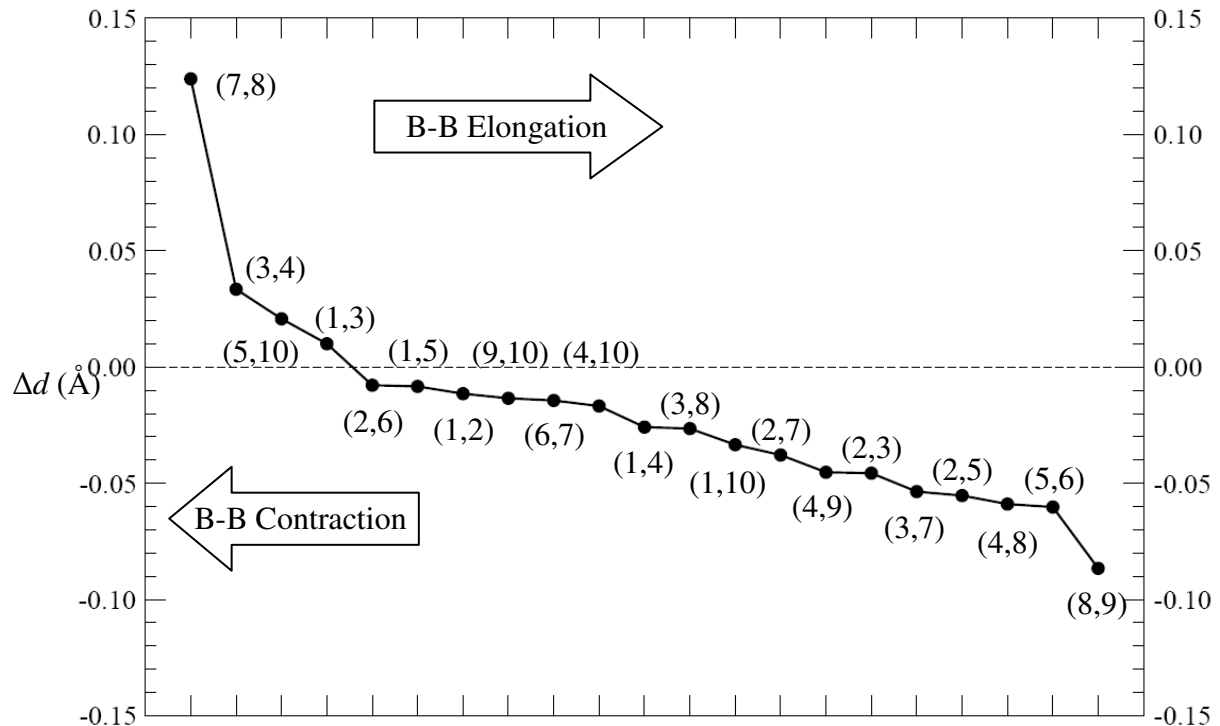
## Analysis of Geometrical Changes on the PEH of *anti*-B<sub>18</sub>H<sub>22</sub> and *syn*-B<sub>18</sub>H<sub>22</sub>

Figure 7a and Figure 7b in the main text display, respectively, the structure and numbering of *anti*-B<sub>18</sub>H<sub>22</sub> ( $C_i$  symmetry) and *syn*-B<sub>18</sub>H<sub>22</sub> ( $C_2$  symmetry) clusters following Lipscomb<sup>14</sup> and Todd.<sup>15</sup> The relation between boron atoms under symmetry operations in these clusters are related by a “primed” number. Figure S5, Figure S6 and Figure S7 gather the distance differences in boron atoms for *anti*-B<sub>18</sub>H<sub>22</sub> when the geometry evolves from S<sub>0</sub> ground state to T<sub>1</sub>, S<sub>1</sub> and (S<sub>0</sub>/S<sub>1</sub>)<sub>CI</sub>, respectively. Figure S8 and Figure S9 display distance differences in boron atoms for *syn*-B<sub>18</sub>H<sub>22</sub> when the geometry evolves from S<sub>0</sub> ground state to T<sub>1</sub> and (S<sub>0</sub>/S<sub>1</sub>)<sub>CI</sub>, respectively.

**Figure S5.** Boron-boron distance differences (in Å) between the energy minima geometries of ground state S<sub>0</sub> and first triplet state T<sub>1</sub> in *anti*-B<sub>18</sub>H<sub>22</sub>.  $\Delta d = d(\text{B-B})_{\text{S}0} - d(\text{B-B})_{\text{T}1}$ . Positive/negative  $\Delta d$  implies bond contraction/elongation when passing from S<sub>0</sub> to T<sub>1</sub>. Atom labels follow from Figure 7 in the main text.



**Figure S6.** Boron-boron distance differences (in Å) between the energy minima geometries of ground state  $S_0$  and first excited singlet state  $S_1$  in *anti*-B<sub>18</sub>H<sub>22</sub>.  $\Delta d = d(\text{B-B})_{S_0} - d(\text{B-B})_{S_1}$ . Positive/negative  $\Delta d$  implies bond contraction/elongation when passing from  $S_0$  to  $S_1$ . Both structures have  $C_i$  symmetry and therefore we display only symmetry-unique B-B distance differences. Atom labels follow from Figure 7 in the main text.



**Figure S7.** Boron-boron distance differences (in Å) between the energy minimum geometry of ground state  $S_0$  and conical intersection geometry  $(S_0/S_1)_{\text{CI}}$  in *anti*-B<sub>18</sub>H<sub>22</sub>.  $\Delta d = d(\text{B-B})_{S_0} - d(\text{B-B})_{S_0/S_1(\text{CI})}$ . Positive/negative  $\Delta d$  implies bond shrinkage/elongation when passing from  $S_0$  to  $(S_0/S_1)_{\text{CI}}$ . Due to their small value, central differences are gathered in a horizontal brace, in increasing order from left to right;  $[\pm]$  in the central list means change of sign in  $d$ , from + to -. Atom labels follow from Figure 7 in the main text.

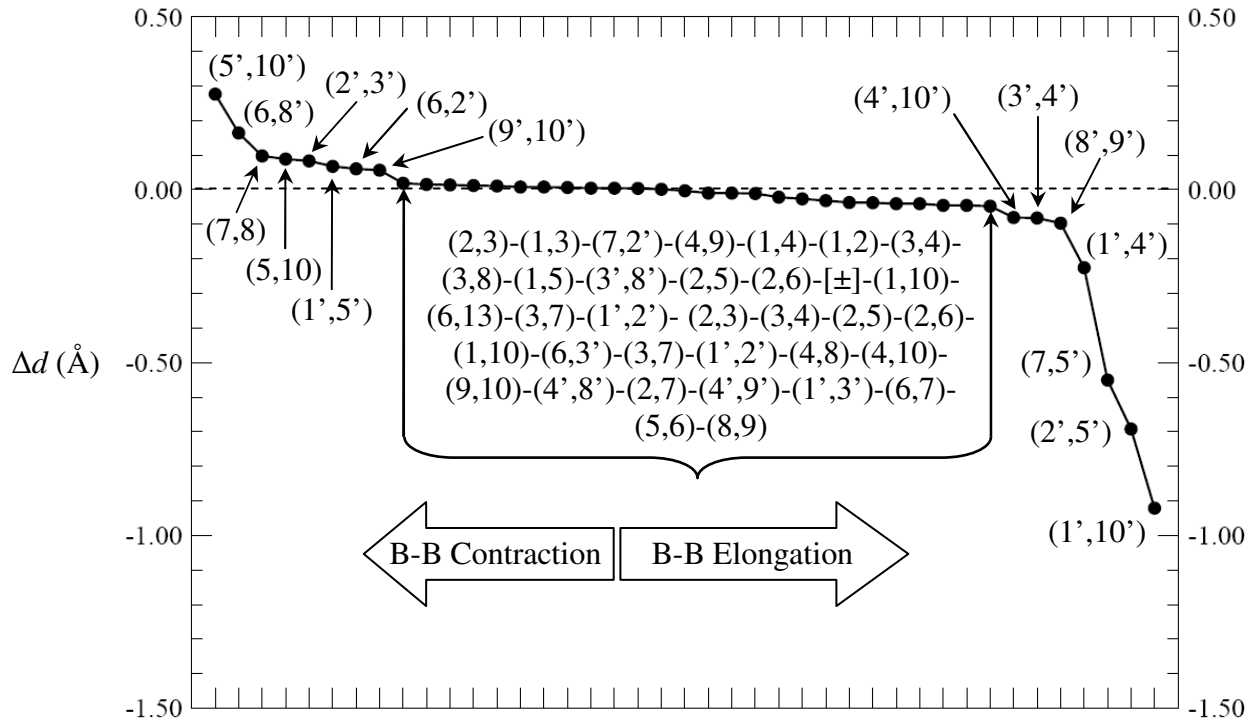


**Figure S8.** Boron-boron distance differences (in Å) between the energy minima geometries of ground state  $S_0$  and first triplet state  $T_1$  in *syn*-B<sub>18</sub>H<sub>22</sub>.  $\Delta d = d(\text{B-B})_{S_0} - d(\text{B-B})_{T_1}$ . Positive/negative  $\Delta d$  implies bond contraction/elongation when passing from  $S_0$  to  $T_1$ . Both structures have C<sub>2</sub> symmetry and therefore we display only symmetry-unique B-B distance differences. Atom labels follow from Figure 7 in the main text.

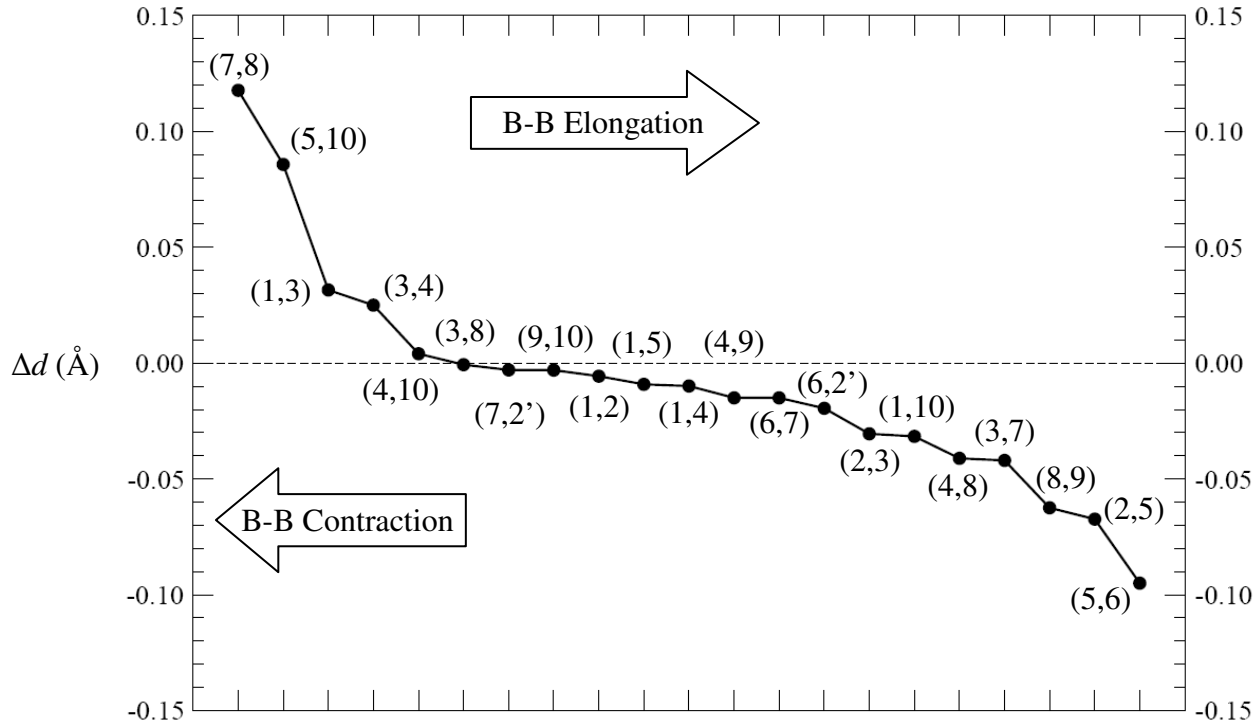


**Figure S9.** Boron-boron distance differences (in Å) between the energy minimum geometry of ground state  $S_0$  and conical intersection geometry ( $S_0/S_1$ )<sub>CI</sub> in *syn*-B<sub>18</sub>H<sub>22</sub>.  $\Delta d = d(\text{B-B})_{S_0} - d(\text{B-B})_{S_0/S_1(\text{CI})}$ . Positive/negative  $\Delta d$  implies bond contraction/elongation when passing from  $S_0$  to ( $S_0/S_1$ )<sub>CI</sub>. Due to their small value, central differences are gathered in a horizontal brace, in increasing order from left to right; [ $\pm$ ] in the central list means change of sign in  $d$ , from + to -. Atom labels follow from Figure 7 in the main text.

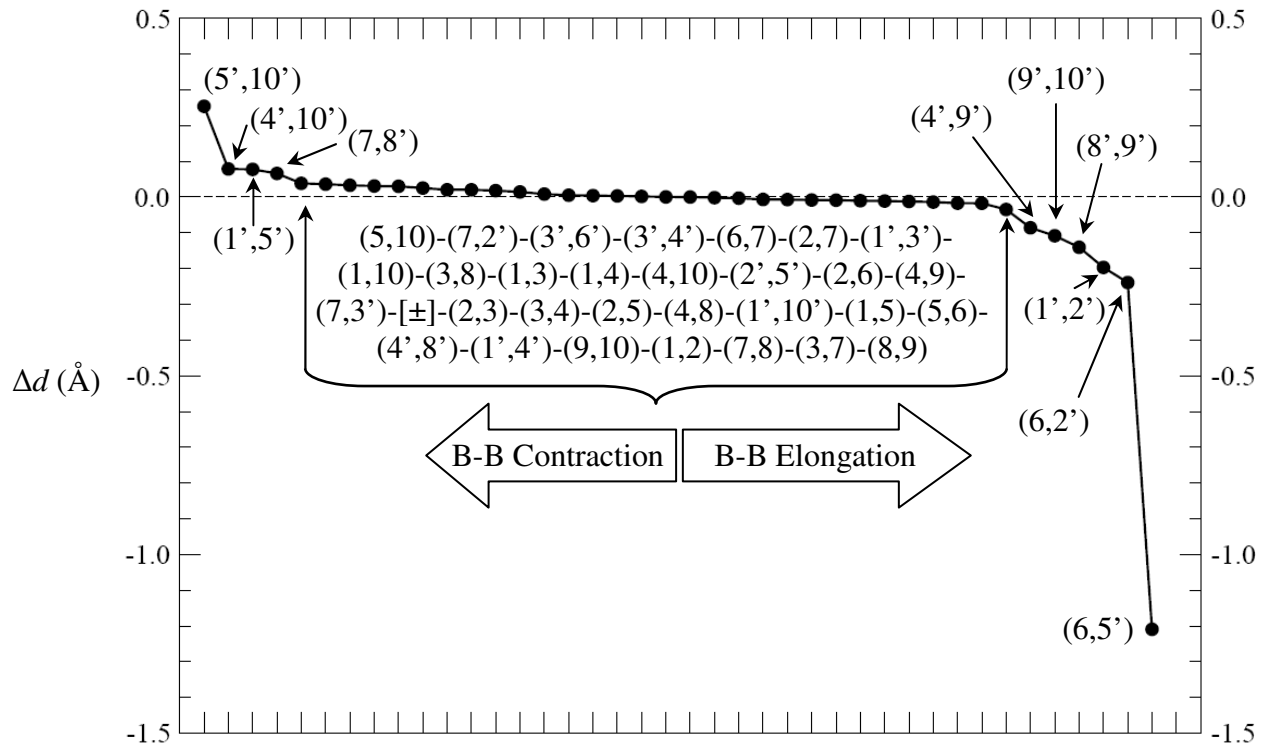


**Table S1.** Theoretical (CASPT2) and experimental absorption spectra of *anti*-B<sub>18</sub>H<sub>22</sub> ( $C_i$ ).

State	CASPT2			Experimental			Main configurations (%) <sup>d</sup>
	E <sub>VA</sub> <sup>a</sup> /eV	$\lambda_{VA}^a$ /nm	f	A <sub>max</sub> <sup>b</sup> /eV	$\lambda_{amax}^b$ /nm	f <sup>c</sup>	
1 <sup>1</sup> A <sub>g</sub>							
1 <sup>1</sup> A <sub>u</sub>	3.93	315	0.265	3.77	329	~0.4	28a <sub>u</sub> → 29a <sub>g</sub> 90
2 <sup>1</sup> A <sub>u</sub>	4.99	248	0.051	4.56	272	~0.2	27a <sub>u</sub> → 29a <sub>g</sub> 74; 28a <sub>u</sub> → 30a <sub>g</sub> 16
2 <sup>1</sup> A <sub>g</sub>	5.12	242	forb.				28a <sub>g</sub> → 29a <sub>g</sub> 90
3 <sup>1</sup> A <sub>g</sub>	5.49	226	forb.				28a <sub>u</sub> → 29a <sub>u</sub> 62; 28a <sub>u</sub> → 30a <sub>u</sub> 21
4 <sup>1</sup> A <sub>g</sub>	5.54	224	forb.				26a <sub>g</sub> → 29a <sub>g</sub> 62; 27a <sub>g</sub> → 29a <sub>g</sub> 21
3 <sup>1</sup> A <sub>u</sub>	5.55	223	0.055				26a <sub>u</sub> → 29a <sub>g</sub> 84
5 <sup>1</sup> A <sub>g</sub>	5.65	219	forb.				28a <sub>u</sub> → 30a <sub>u</sub> 54; 28a <sub>u</sub> → 29a <sub>u</sub> 16
4 <sup>1</sup> A <sub>u</sub>	5.85	212	0.884	5.76	215	~1.0	28a <sub>u</sub> → 30a <sub>g</sub> 70; 27a <sub>u</sub> → 29a <sub>g</sub> 15
6 <sup>1</sup> A <sub>g</sub>	5.92	209	forb.				27a <sub>g</sub> → 29a <sub>g</sub> 47; 26a <sub>g</sub> → 29a <sub>g</sub> 23
7 <sup>1</sup> A <sub>g</sub>	6.58	188	forb.				27a <sub>u</sub> → 29a <sub>u</sub> 68
5 <sup>1</sup> A <sub>u</sub>	6.65	186	0.094				28a <sub>g</sub> → 29a <sub>u</sub> 56; 27a <sub>u</sub> → 30a <sub>g</sub> 25
6 <sup>1</sup> A <sub>u</sub>	6.76	183	0.746				27a <sub>u</sub> → 30a <sub>g</sub> 48; 28a <sub>g</sub> → 29a <sub>u</sub> 24
1 <sup>3</sup> A <sub>u</sub>	3.48	356	–				28a <sub>u</sub> → 29a <sub>g</sub> 90
2 <sup>3</sup> A <sub>u</sub>	4.63	268	forb. <sup>e</sup>				27a <sub>u</sub> → 29a <sub>g</sub> 90
1 <sup>3</sup> A <sub>g</sub>	4.64	267	0.008 <sup>e</sup>				28a <sub>g</sub> → 29a <sub>g</sub> 69; 28a <sub>u</sub> → 29a <sub>u</sub> 23
2 <sup>3</sup> A <sub>g</sub>	5.16	240	0.072 <sup>e</sup>				28a <sub>u</sub> → 29a <sub>u</sub> 30; 26a <sub>g</sub> → 29a <sub>g</sub> 28
3 <sup>3</sup> A <sub>g</sub>	5.28	235	0.003 <sup>e</sup>				28a <sub>u</sub> → 30a <sub>u</sub> 80
3 <sup>3</sup> A <sub>u</sub>	5.43	228	forb. <sup>e</sup>				28a <sub>u</sub> → 30a <sub>g</sub> 87
4 <sup>3</sup> A <sub>u</sub>	5.56	223	forb. <sup>e</sup>				26a <sub>u</sub> → 29a <sub>g</sub> 74; 28a <sub>g</sub> → 29a <sub>u</sub> 14
4 <sup>3</sup> A <sub>g</sub>	5.61	221	0.216 <sup>e</sup>				27a <sub>g</sub> → 29a <sub>g</sub> 63; 28a <sub>u</sub> → 29a <sub>u</sub> 13
5 <sup>3</sup> A <sub>g</sub>	5.76	215	0.147 <sup>e</sup>				26a <sub>g</sub> → 29a <sub>g</sub> 45; 28a <sub>u</sub> → 29a <sub>u</sub> 23

<sup>a</sup> Computed vertical absorption energy (E<sub>VA</sub>) and vertical wavelength ( $\lambda_{VA}$ ).

<sup>b</sup> Experimental absorption band maxima energy (A<sub>max</sub>) and wavelength band maxima ( $\lambda_{amax}$ ) in hexane.

<sup>c</sup> Normalized using molar absorption coefficients.

<sup>d</sup> 27a<sub>u</sub> (HOMO-1), 28a<sub>u</sub> (HOMO), 29a<sub>g</sub> (LUMO), 30a<sub>g</sub> (LUMO+1).

<sup>e</sup> Triplet(1<sup>3</sup>A<sub>u</sub>) – triplet oscillator strengths.

**Table S2.** Theoretical (CASPT2) and experimental absorption spectra of *syn*-B<sub>18</sub>H<sub>22</sub> (*C*<sub>2</sub>).

State	CASPT2			$\mu$ /D	Experimental			Main configurations (%) <sup>d</sup>
	E <sub>VA</sub> <sup>a</sup> /eV	$\lambda_{VA}^a$ /nm	f		A <sub>max</sub> <sup>b</sup> /eV	$\lambda_{amax}^b$ /nm	f <sup>c</sup>	
1 <sup>1</sup> A				2.45				
1 <sup>1</sup> B	4.26	291	0.338	2.12	4.03	308	~0.6	29a → 28b 85
2 <sup>1</sup> A	4.65	267	0.073	1.45				27b → 28b 81
3 <sup>1</sup> A	5.17	240	0.034	1.39				29a → 30a 34; 26b → 28b 34
2 <sup>1</sup> B	5.28	235	0.017	1.32				28a → 28b 80
4 <sup>1</sup> A	5.56	223	0.158	0.25	5.41	229	~0.5	29a → 30a 40; 26b → 28b 20
3 <sup>1</sup> B	5.76	215	0.251	1.35	5.41	229	~0.5	27b → 30a 74
5 <sup>1</sup> A	5.84	212	0.004	0.72				25b → 28b 57; 26b → 28b 28
4 <sup>1</sup> B	5.91	210	0.027	0.17				27a → 28b 63
6 <sup>1</sup> A	6.43	193	0.041	3.24				29a → 31a 80
5 <sup>1</sup> B	6.50	191	0.156	2.30	>6.2	<200	~0.9	27b → 31a 66
6 <sup>1</sup> B	6.55	189	0.212	7.41	>6.2	<200	~0.9	29b → 32a 47; 26b → 30a 35
7 <sup>1</sup> A	6.56	189	0.159	7.41	>6.2	<200	~0.9	28a → 30a 51; 29a → 32a 33
1 <sup>3</sup> B	3.76	329	–	2.29				29a → 28b 91
1 <sup>3</sup> A	4.13	300	0.003 <sup>e</sup>	2.69				27b → 28b 90
2 <sup>3</sup> A	4.95	250	0.007 <sup>e</sup>	0.96				29a → 30a 56; 26b → 28b 28
2 <sup>3</sup> B	5.09	243	0.001 <sup>e</sup>	1.02				28b → 30a 44; 28a → 30a 42
3 <sup>3</sup> A	5.19	239	0.032 <sup>e</sup>	2.09				25b → 28b 32; 26b → 28b 24
3 <sup>3</sup> B	5.46	227	0.003 <sup>e</sup>	1.62				28a → 30b 37; 27b → 30a 34
4 <sup>3</sup> B	5.57	223	0.021 <sup>e</sup>	6.63				27a → 30b 53; 26b → 30a 20
4 <sup>3</sup> A	5.71	217	0.009 <sup>e</sup>	0.34				25b → 28b 51; 26a → 28a 16
5 <sup>3</sup> A	6.08	204	0.105 <sup>e</sup>	1.43				27b → 29b 43; 26b → 28b 18

<sup>a</sup> Computed vertical absorption energy (E<sub>VA</sub>) and vertical wavelength ( $\lambda_{VA}$ ).

<sup>b</sup> Experimental absorption band maxima energy (A<sub>max</sub>) and wavelength band maxima ( $\lambda_{amax}$ ) in hexane.

<sup>c</sup> Normalized to the 215 nm band of the *anti* isomer using molar absorption coefficients.

<sup>d</sup> 27b (HOMO-1), 29a (HOMO), 28b (LUMO), 30a (LUMO+1).

<sup>e</sup> Triplet(1<sup>3</sup>B) – triplet oscillator strengths.

**Table S3.** Cartesian coordinates (Å) of the DFT/B3LYP and CASSCF(12/12) optimized structures obtained in the paper and absolute CASSCF(12/12) energies for the corresponding state. 6-31+G(d) basis set

---

Atom	x	y	z
<i>anti</i> -B <sub>18</sub> H <sub>22</sub> CASSCF(12/12)//B3LYP S <sub>0</sub> minimum E = -457.050424 au			
B	0.234986	-0.700197	0.523689
B	-0.234946	0.700052	-0.523739
B	0.590982	1.001299	1.002861
B	-0.591048	-1.001487	-1.002804
B	2.326294	1.189951	0.781225
B	-2.326371	-1.189996	-0.781088
B	1.245844	1.765672	-0.477559
B	2.964975	0.850832	-0.811482
B	3.227034	-0.327270	0.527634
B	1.682032	-0.343396	1.449578
B	-1.682012	0.343242	-1.449614
B	-3.227030	0.327273	-0.527658
B	-2.964885	-0.850642	0.811647
B	-1.245911	-1.765690	0.477726
B	2.009087	-1.599267	0.278705
B	2.972280	-0.933163	-1.062618
B	-2.009088	1.599303	-0.278951
B	-2.972235	0.933405	1.062490
H	0.065376	1.593658	1.886390
H	1.148115	2.918074	-0.739012
H	3.817448	1.487499	-1.336062
H	4.256140	-0.479815	1.098424
H	1.689931	-0.685491	2.588115
H	-0.065504	-1.593975	-1.886286
H	-1.689883	0.685212	-2.588189
H	-4.256150	0.479744	-1.098442
H	-3.817371	-1.487119	1.336438
H	-1.148322	-2.918118	0.739121
H	2.859386	2.064326	1.383904
H	-2.859528	-2.064404	-1.383659
H	2.078502	-2.747047	0.569092
H	3.698014	-1.531159	-1.784203
H	-2.078464	2.747003	-0.569667
H	-3.697994	1.531373	1.784074
H	1.825311	-1.582252	-1.029475
H	2.452027	0.083830	-1.757220
H	0.658529	1.115586	-1.444457
H	-1.825390	1.582699	1.029225
H	-2.451736	-0.083465	1.757113
H	-0.658379	-1.115768	1.444556

**Table S3** (continuation).anti-B<sub>18</sub>H<sub>22</sub> CASSCF(12/12) S<sub>1</sub> minimum E = -456.881618 au

B	0.277465	-0.715589	0.493648
B	-0.277465	0.715589	-0.493648
B	0.592094	1.021237	1.016843
B	-0.592094	-1.021237	-1.016843
B	2.336705	1.208592	0.776470
B	-2.336705	-1.208592	-0.776470
B	1.282373	1.773891	-0.520278
B	-1.282373	-1.773891	0.520278
B	2.973147	0.848978	-0.849345
B	-2.973147	-0.848978	0.849345
B	3.231670	-0.339116	0.504283
B	-3.231670	0.339116	-0.504283
B	1.751163	-0.327026	1.466559
B	-1.751163	0.327026	-1.466559
B	1.918635	-1.596821	0.238530
B	-1.918635	1.596821	-0.238530
B	2.996623	-0.942734	-1.138609
B	-2.996623	0.942734	1.138609
H	0.073325	1.515213	1.954499
H	-0.073325	-1.515213	-1.954499
H	1.190210	2.912716	-0.812185
H	-1.190210	-2.912716	0.812185
H	3.843678	1.479979	-1.335618
H	-3.843678	-1.479979	1.335618
H	4.270426	-0.514938	1.039377
H	-4.270426	0.514938	-1.039377
H	1.733177	-0.618993	2.610787
H	-1.733177	0.618993	-2.610787
H	2.896012	2.075986	1.355367
H	-2.896012	-2.075986	-1.355367
H	1.994081	-2.737514	0.531195
H	-1.994081	2.737514	-0.531195
H	3.849264	-1.519197	-1.713800
H	-3.849264	1.519197	1.713800
H	1.916005	-1.612487	-1.144848
H	-1.916005	1.612487	1.144848
H	2.491775	0.050171	-1.823487
H	-2.491775	-0.050171	1.823487
H	0.580401	1.091642	-1.412382
H	-0.580401	-1.091642	1.412382

**Table S3** (continuation).anti-B<sub>18</sub>H<sub>22</sub> CASSCF(12/12)//B3LTP T<sub>1</sub> minimum E = -456.924191 au

B	0.255827	-0.71494	0.518818
B	-0.255827	0.71494	-0.518818
B	0.579807	1.016719	0.995776
B	-0.579807	-1.016719	-0.995776
B	2.312165	1.196532	0.803079
B	-2.312165	-1.196532	-0.803079
B	1.311926	1.738628	-0.542598
B	-1.311926	-1.738628	0.542598
B	2.955933	0.82682	-0.818519
B	-2.955933	-0.82682	0.818519
B	3.196705	-0.345062	0.545546
B	-3.196705	0.345062	-0.545546
B	1.709791	-0.312008	1.488271
B	-1.709791	0.312008	-1.488271
B	1.877287	-1.595461	0.289411
B	-1.877287	1.595461	-0.289411
B	2.981028	-0.965216	-1.067395
B	-2.981028	0.965216	1.067395
H	0.034149	1.545358	1.907309
H	-0.034149	-1.545358	-1.907309
H	1.234274	2.876803	-0.865908
H	-1.234274	-2.876803	0.865908
H	3.829982	1.457419	-1.314601
H	-3.829982	-1.457419	1.314601
H	4.230271	-0.522612	1.100645
H	-4.230271	0.522612	-1.100645
H	1.690685	-0.58701	2.643226
H	-1.690685	0.58701	-2.643226
H	2.866762	2.065582	1.397576
H	-2.866762	-2.065582	-1.397576
H	1.949669	-2.737737	0.602905
H	-1.949669	2.737737	-0.602905
H	3.824357	-1.576631	-1.633914
H	-3.824357	1.576631	1.633914
H	1.889011	-1.639138	-1.080493
H	-1.889011	1.639138	1.080493
H	2.507122	-0.009456	-1.806437
H	-2.507122	0.009456	1.806437
H	0.609793	1.046026	-1.438875
H	-0.609793	-1.046026	1.438875

**Table S3** (continuation).

*anti*-B<sub>18</sub>H<sub>22</sub> CASSCF(12/12) (S<sub>0</sub>/S<sub>1</sub>)<sub>CI</sub> E = -456.864314 au (S<sub>0</sub>)

B	0.178883	0.655119	-0.563162
B	-0.178780	-0.696507	0.657377
B	0.605409	-1.110102	-0.863700
B	-0.369087	0.987824	1.062786
B	2.351528	-1.205912	-0.762628
B	-2.056953	1.515388	0.971557
B	1.401164	-1.696948	0.624227
B	3.004259	-0.714550	0.787603
B	3.155674	0.370695	-0.677150
B	1.587006	0.204976	-1.526520
B	-1.539944	-0.119182	1.620305
B	-3.061801	-0.162478	0.515264
B	-3.111783	0.481999	-1.253550
B	-1.982275	1.630182	-0.711251
B	1.840733	1.586822	-0.497291
B	2.983894	1.117597	0.850042
B	-1.833933	-1.497518	0.593946
B	-2.948608	-1.217397	-0.890537
H	0.058234	-1.775580	-1.612065
H	1.357319	-2.795121	0.948914
H	3.915481	-1.220066	1.268993
H	4.113310	0.526255	-1.283208
H	1.526664	0.412922	-2.651908
H	0.206779	1.604562	1.837171
H	-1.645118	-0.409371	2.728137
H	-4.043832	0.080388	1.079012
H	-4.107798	0.752299	-1.775488
H	-1.860842	2.675578	-1.200080
H	2.873193	-2.079859	-1.291394
H	-2.633082	2.227118	1.669930
H	1.896800	2.661013	-0.901102
H	3.779922	1.757143	1.373585
H	-2.043846	-2.483938	1.148409
H	-3.739597	-2.022377	-1.116480
H	1.864577	1.745252	0.856756
H	2.541152	0.173291	1.663812
H	0.806981	-1.008858	1.542445
H	-1.757464	-1.790568	-0.684177
H	-2.542857	-0.622958	-1.944199
H	-0.692907	0.942843	-1.343655

**Table S3** (continuation).

*syn*-B<sub>18</sub>H<sub>22</sub> CASSCF(12/12)//B3LYP S<sub>0</sub> minimum E = -457.044363 au

B	0.000000	0.000000	-0.598015
B	0.000000	0.000000	1.215547
B	0.916393	1.226742	0.409119
B	-0.916393	-1.226742	0.409119
B	0.000000	2.724253	0.322383
B	0.000000	-2.724253	0.322383
B	-0.180451	1.707751	1.745980
B	-1.665339	2.656552	0.882667
B	-1.304312	2.742830	-0.881213
B	0.132521	1.687002	-1.131430
B	0.180451	-1.707751	1.745980
B	1.665339	-2.656552	0.882667
B	1.304312	-2.742830	-0.881213
B	-0.132521	-1.687002	-1.131430
B	-1.461239	1.066416	-1.470864
B	-2.649379	1.801413	-0.363776
B	1.461239	-1.066416	-1.470864
B	2.649379	-1.801413	-0.363776
H	2.099735	1.261145	0.510997
H	0.205580	2.047702	2.815159
H	-2.185501	3.513368	1.517478
H	-1.450973	3.712035	-1.550298
H	0.825368	1.889285	-2.074195
H	-2.099735	-1.261145	0.510997
H	-0.205580	-2.047702	2.815159
H	2.185501	-3.513368	1.517478
H	1.450973	-3.712035	-1.550298
H	-0.825368	-1.889285	-2.074195
H	0.585874	3.735073	0.540306
H	-0.585874	-3.735073	0.540306
H	-1.800516	0.716542	-2.551411
H	-3.807357	1.954938	-0.565214
H	1.800516	-0.716542	-2.551411
H	3.807357	-1.954938	-0.565214
H	-2.355236	0.547118	-0.643705
H	-2.486499	1.618997	0.946407
H	2.355236	-0.547118	-0.643705
H	2.486499	-1.618997	0.946407
H	-0.928211	0.655434	1.946312
H	0.928211	-0.655434	1.946312

**Table S3** (continuation).

*syn*-B<sub>18</sub>H<sub>22</sub> CASSCF(12/12)//B3LYP T<sub>1</sub> minimum E = -456.904238 au

B	0.000000	0.000000	-0.607788
B	0.000000	0.000000	1.220788
B	0.908810	1.243971	0.390434
B	-0.908810	-1.243971	0.390434
B	0.000000	2.749433	0.258666
B	0.000000	-2.749433	0.258666
B	-0.256938	1.804235	1.730218
B	0.256938	-1.804235	1.730218
B	-1.679030	2.680668	0.875299
B	1.679030	-2.680668	0.875299
B	-1.360848	2.692950	-0.894761
B	1.360848	-2.692950	-0.894761
B	0.102220	1.724768	-1.167767
B	-0.102220	-1.724768	-1.167767
B	-1.438700	0.939903	-1.396552
B	1.438700	-0.939903	-1.396552
B	-2.683943	1.741195	-0.295936
B	2.683943	-1.741195	-0.295936
H	2.082083	1.300460	0.559427
H	-2.082083	-1.300460	0.559427
H	0.100795	2.120755	2.814185
H	-0.100795	-2.120755	2.814185
H	-2.180670	3.574179	1.475038
H	2.180670	-3.574179	1.475038
H	-1.579327	3.617796	-1.605696
H	1.579327	-3.617796	-1.605696
H	0.803828	1.949798	-2.096835
H	-0.803828	-1.949798	-2.096835
H	0.578977	3.776101	0.421028
H	-0.578977	-3.776101	0.421028
H	-1.804134	0.547220	-2.454251
H	1.804134	-0.547220	-2.454251
H	-3.828992	1.922450	-0.543938
H	3.828992	-1.922450	-0.543938
H	-2.392908	0.502488	-0.535490
H	2.392908	-0.502488	-0.535490
H	-2.520013	1.628631	1.000074
H	2.520013	-1.628631	1.000074
H	-0.891179	0.536834	1.935948
H	0.891179	-0.536834	1.935948

**Table S3** (continuation).

*syn*-B<sub>18</sub>H<sub>22</sub> CASSCF(12/12) (S<sub>0</sub>/S<sub>1</sub>)<sub>CI</sub> E = -456.911466 au

B	0.159262	0.060743	-0.419640
B	0.318228	0.323952	1.337267
B	0.989114	1.508889	0.274287
B	-0.630920	-1.218913	0.563370
B	-0.085480	2.900135	0.053895
B	-0.165516	-2.988213	-0.124409
B	-0.077629	2.064704	1.610784
B	-0.122276	-2.644472	1.520536
B	-1.649160	2.832803	0.809453
B	1.354650	-3.061686	0.770589
B	-1.497896	2.617718	-0.968615
B	1.407765	-2.670197	-0.907296
B	0.008603	1.659552	-1.214189
B	0.053305	-1.555949	-1.141765
B	-1.514344	0.848439	-1.245140
B	1.638786	-0.917251	-1.212152
B	-2.690079	1.691548	-0.145191
B	2.685686	-1.870377	0.089356
H	2.122798	1.668795	0.233255
H	-1.701076	-1.157221	1.001610
H	0.290612	2.527819	2.596379
H	-0.661302	-2.998024	2.471993
H	-2.144796	3.734662	1.322643
H	1.872738	-3.860206	1.428307
H	-1.801707	3.392736	-1.755858
H	1.736813	-3.419980	-1.710185
H	0.554399	1.770810	-2.218095
H	-0.594363	-1.575469	-2.088433
H	0.419856	3.932278	0.072674
H	-0.917585	-3.766494	-0.519409
H	-1.941568	0.341888	-2.183547
H	2.065532	-0.550940	-2.214557
H	-3.830786	1.734856	-0.284215
H	3.741252	-2.151920	-0.272891
H	-2.286012	0.444013	-0.232910
H	2.435275	-0.570646	-0.293287
H	-2.396378	1.772074	1.135295
H	2.606969	-1.611486	1.231010
H	-0.710059	0.939511	1.906151
H	0.957289	-0.178479	2.149868

## References

---

- (1) Andersson, K.; Malmqvist, P.-Å.; Roos, B. O. *J. Chem. Phys.* **1992**, *96*, 1218-1226.
- (2) Roos, B. O.; Fülscher, M. P.; Malmqvist, P.-Å.; Serrano-Andrés, L.; Pierloot, K.; Merchán, M. *Adv. Chem. Phys.* **1996**, *93*, 219-331.
- (3) Merchán, M.; Serrano-Andrés, L.; Fülscher, M. P.; Roos, B. O. In: *Recent Advances in Multireference Methods*. Hirao, K. Ed; World Scientific Publishing, Singapore, **1999**.
- (4) Merchán, M.; Serrano-Andrés, L. In: *Computational Photochemistry*; Olivucci, M. Ed; Elsevier Publishing: Amsterdam, **2005**
- (5) Malmqvist, P.-Å.; Rendell, A.; Roos, B. O. *J. Phys. Chem.*, **1990**, *94*, 5477-5482.
- (6) Ghigo, G.; Roos, B. O.; Malmqvist, P.-Å. *Chem. Phys. Lett.* **2004**, *396*, 142-149.
- (7) Forsberg, J.; Malmqvist, P.-Å. *Chem. Phys. Lett.* **1997**, *274*, 196-204.
- (8) Aquilante, F. ; De Vico, L. ; Ferré, N. ; Ghigo, G. ; Malmqvist, P.- Å.; Pedersen, T.; Pitonak, M.; Reiher, M.; Roos, B. O.; Serrano-Andrés, L.; Urban, M.; Veryazov, V.; Lindh, R. *J. Comp. Chem.* **2010**, *31*, 224-247.
- (9) Frisch, M. J.; Trucks, G. W.; Schlegel, H. B.; Scuseria, G. E.; Robb, M. A.; Cheeseman, J. R.; Montgomery, J. A., Jr.; Vreven, T.; Kudin, K. N.; Burant, J. C.; Millam, J. M.; Iyengar, S. S.; Tomasi, J.; Barone, V.; Mennucci, B.; Cossi, M.; Scalmani, G.; Rega, N.; Petersson, G. A.; Nakatsuji, H.; Hada, M.; Ehara, M.; Toyota, K.; Fukuda, R.; Hasegawa, J.; Ishida, M.; Nakajima, T.; Honda, Y.; Kitao, O.; Nakai, H.; Klene, M.; Li, X.; Knox, J. E.; Hratchian, H. P.; Cross, J. B.; Bakken, V.; Adamo, C.; Jaramillo, J.; Gomperts, R.; Stratmann, R. E.; Yazyev, O.; Austin, A. J.; Cammi, R.; Pomelli, C.; Ochterski, J. W.; Ayala, P. Y.; Morokuma, K.; Voth, G. A.; Salvador, P.; Dannenberg, J. J.; Zakrzewski, V. G.; Dapprich, S.; Daniels, A. D.; Strain, M. C.; Farkas, O.; Malick, D. K.; Rabuck, A. D.; Raghavachari, K.; Foresman, J. B.; Ortiz, J. V.; Cui, Q.; Baboul, A. G.; Clifford, S.; Cioslowski, J.; Stefanov, B. B.; Liu, G.; Liashenko, A.; Piskorz, P.; Komaromi, I.; Martin, R. L.; Fox, D. J.; Keith, T.; Al-Laham, M. A.; Peng, C. Y.; Nanayakkara, A.; Challacombe, M.; Gill, P. M. W.; Johnson, B.; Chen, W.; Wong, M. W.; Gonzalez, C.; Pople, J. A. *Gaussian 03*, Inc.: Wallingford CT, **2004**.
- (10) De Vico, L.; Olivucci, M.; Lindh, R. *J. Chem. Theory Comp.* **2005**, *1*, 1029-1037.
- (11) Malmqvist, P. A.; Roos, B. O.; Schimmelpfennig, B. *Chem. Phys. Lett.* **2002**, *357*, 230-240.
- (12) Strickler, S. J.; Berg, R. A. *J. Chem. Phys.* **1962**, *37*, 814.
- (13) Rubio-Pons, O.; Serrano-Andrés, L.; Merchán, M. *J. Phys. Chem. A* **2001**, *105*, 9664-9676.
- (14) Simpson, P. G.; Lipscomb, W. N. *Proc. Nat. Acad. Sci.* **1962**, *48*, 1490-1491.
- (15) Todd, L. *J. Pure Appl. Chem.* **1972**, *30*, 587-606.